

Neural network variational Monte Carlo for positronic chemistry

Gino Cassella^{1*}, W.M.C. Foulkes¹, David Pfau^{2,1}, and James S. Spencer²
¹*Dept. of Physics, Imperial College London, London SW7 2AZ, United Kingdom and*
²*DeepMind, London NIC 4DJ, United Kingdom*
(*g.cassella20@imperial.ac.uk)
(Dated: February 8, 2024)

Quantum chemical calculations of the ground-state properties of positron-molecule complexes are challenging. The main difficulty lies in employing an appropriate basis set for representing the coalescence between electrons and a positron. Here, we tackle this problem with the recently developed Fermionic neural network (FermiNet) wavefunction, which does not depend on a basis set. We find that FermiNet produces highly accurate, in some cases state-of-the-art, ground-state energies across a range of atoms and small molecules with a wide variety of qualitatively distinct positron binding characteristics. We calculate the binding energy of the challenging non-polar benzene molecule, finding good agreement with the experimental value, and obtain annihilation rates which compare favourably with those obtained with explicitly correlated Gaussian wavefunctions. Our results demonstrate a generic advantage of neural network wavefunction-based methods and broaden their applicability to systems beyond the standard molecular Hamiltonian.

The positron – the positively charged anti-particle of the electron – was first postulated by Dirac [1] almost a century ago. Today, the once exotic notion of anti-matter is technologically relevant in a variety of fields, such as medical physics [2], astrophysics [3], and materials science [4, 5].

Experimental apparatus for trapping large numbers of positrons continues to grow in sophistication, offering a glimpse into a world of exotic antimatter chemistry [6]. These advances motivate the development of improved computational tools able to describe positronic bound states and thus accelerate the continued development of new antimatter-based technologies. In the present work, we make progress in this direction by developing a highly accurate method for the *ab initio* calculation of the ground-state properties of bound states between positrons and ordinary molecules.

Despite annihilating upon contact with an electron, positrons readily form bound states with ordinary molecules. The formation of these bound states, enabled by an incident positron exciting a vibrational Feshbach resonance, results in greatly enhanced annihilation rates. This process has recently been successfully exploited in positron annihilation spectroscopy experiments [7–14], where the energy-dependent annihilation rate enables sensitive measurements of the positron binding energy [15].

Theoretical calculations of positron binding energies and annihilation rates have been performed using many of the standard tools of computational chemistry. Positron binding to atoms and molecules has been studied using wavefunction expansions in explicitly correlated Gaussians with the stochastic variational method (ECG-SVM) [16–24], configuration interaction (CI) methods [25–31], and quantum Monte Carlo (QMC) methods [32–40]. The annihilation rate and lifetime of positrons in solids, particularly in the presence of defects, has been studied using density functional theory [41, 42] and quantum Monte Carlo methods [43, 44].

Despite the intense theoretical interest, describing the positronic wavefunction remains challenging for several reasons. As a result of the strong correlations enabled by the attractive interaction between electrons and the positron, molecular bound states often resemble a ‘virtual’ positronium atom

weakly bound to the molecule [45]. Due to the repulsive potential between the nuclei of the host molecule and the positron, these virtual atoms are localized away from the nucleus. Accurately describing such a wavefunction (particularly the electron-positron cusp) in a basis of single-particle orbitals centred on the nuclei requires the inclusion of basis functions with very large angular momenta [46]. This results in very slow convergence of CI calculations with the maximum angular momentum of functions included in the basis. Furthermore, the positronic density is typically highly diffuse, requiring the augmentation of standard basis sets with additional diffuse basis functions [27, 29–31].

The most successful description of positron binding to molecules comes from a recent work that develops a many-body theory of positron binding to molecules and produces positron binding energies in close agreement with experimental measurements [47]. In their work, Hofierka *et al.* highlight the shortcomings of QMC methods applied to positron binding, particularly the lack of calculations for large non-polar molecules, which constitute the majority of experimentally studied systems [15]. Here, we address this shortcoming.

We propose a new approach to calculating the ground state properties of molecular positronic bound states, based on recently developed neural network wavefunction ansätze for QMC [48]. The Fermionic neural network (FermiNet) models the many-body wavefunction without referencing a set of basis functions. This conveniently sidesteps a number of the aforementioned difficulties in describing positronic wavefunctions. We extend FermiNet to represent the positronic component of the wavefunction on an even footing with the electronic component. With a minimal alteration to the neural network architecture, we obtain a flexible and accurate ansatz for mixed electron-positron wavefunctions. We calculate positron binding energies and annihilation rates for a range of systems with qualitatively distinct mechanisms for positron binding and obtain state-of-the-art accuracy for the ground-state energy in these systems. Our method yields a positron binding energy for benzene in close agreement with the experimental value and the many-body theory of Hofierka *et al.* [47], and we obtain annihilation rates which compare favourably with

highly accurate ECG-SVM calculations for alkali metal atoms and small molecules.

RESULTS

We benchmark the accuracy of FermiNet in calculations of the ground-state energy, the positron binding energy, and the positron annihilation rate for a series of well-studied positronic systems. These are presented here in (approximate) order of increasing complexity. Unless otherwise specified, all results presented herein were obtained using the network architecture and training protocol detailed by Spencer [49]. We pre-train the electron orbitals to the Hartree-Fock solution of the bare molecule and do not pre-train the positron orbitals. Errors in energy expectation values are evaluated using a re-blocking approach [50] to account for sequential correlations in the Metropolis-Hastings sampling.

Binding energies

Positronium hydride – The positronium (Ps) atom (consisting of a bound electron and positron) and hydrogen form a stable molecule. Here we work within the Born-Oppenheimer approximation, neglecting the proton’s motion. Almost exact ECG calculations are available for this system [16], yielding a ground-state energy of $E_0 = -0.7891794$ Hartrees. We obtain a ground state energy of $E_0 = -0.789144(3)$ Hartrees.

Sodium and magnesium atoms – The first ionisation energy of sodium, 0.1886 Hartrees, is smaller than the binding energy of the Ps atom, 0.25 Hartrees. The positronic sodium atom is then more accurately described as a bound complex of a positronium atom and a sodium cation. The binding energy of this complex is calculated as $\epsilon = E([\text{Na}^+, \text{Ps}]) - E(\text{Na}^+) - 0.25$. We fail to predict binding without variance matching, obtaining $\epsilon = -0.37$ milliHartrees. Utilizing a variance matching procedure, we obtain $\epsilon = 0.32(15)$ milliHartrees, predicting binding in agreement with previous ECG-FCSVM ($\epsilon_{\text{FCSVM}} = 0.473$ milliHartrees [51]) calculations.

We obtain a positron binding energy of 0.01618(9) Hartrees for the magnesium atom. This agrees with previous ECG-FCSVM (0.016930 Hartrees [28]) and CI (0.017099 Hartrees [28]) results.

Lithium hydride and beryllium oxide – We have calculated the ground-state energy of LiH and its positronic complex for a range of interatomic separations (see Data Tables in Supplementary Material). Fitting these potential energy surfaces using Nesterov’s algorithm, implemented in the MOLCAS package, we obtain equilibrium bond distances of 3.0196 Bohr, with ground-state energy -8.07050(1) Hartrees for LiH, and 3.371 Bohr with a ground state energy of -8.10774(1) Hartrees for $[\text{LiH}, e^+]$. These deviate very slightly from the widely accepted literature values of 3.015 Bohr (LiH) and 3.348 Bohr ($[\text{LiH}, e^+]$). We have calculated ground-state energies at the canonical separations for comparison with previous results, shown in Table I. Our calculations are not only in excellent

agreement with previous work but are seen to yield the most accurate variational result for $[\text{LiH}, e^+]$.

We have calculated the ground-state wavefunction of BeO over a range of interatomic separations – from below the equilibrium separation to dissociation. We fit the potential energy surfaces using MOLCAS and obtain an equilibrium bond distance of 2.515 Bohr with a ground-state energy of -89.90572(4) Hartrees for BeO, and 2.530 Bohr with a ground-state energy of -89.93082(3) Hartrees for $[\text{BeO}, e^+]$. We compare our results against previous calculations in Table I and find that FermiNet yields the most accurate variational result for $[\text{BeO}, e^+]$.

The electronic ground state of BeO transitions from the spin-singlet configuration at the equilibrium interatomic separation to the spin-triplet configuration at the dissociative limit. We enforce the appropriate ground-state spin configuration by choosing $S_z = 1$ (as FermiNet is a spin-assigned wavefunction) at wide interatomic separations. The resulting potential energy surfaces are plotted in Fig. 1. At ~ 4 Bohr, the electronic ground-state transitions between the spin-singlet and spin-triplet, causing a sharp change in the ground-state dipole moment and the resulting positron binding energy with the molecular ground-state, which vanishes almost completely. At ~ 6 Bohr, we see a smooth transition between two qualitatively distinct binding modes between the molecule and the positron – binding to the molecular dipole field below this separation and binding exclusively to the ‘lone’ beryllium atom beyond this separation. This is readily seen by visualizing the ground-state positron density on either side of the maximum, as shown in Fig. 1 for the triplet state, and corroborated by the dipole moment falling below the critical threshold for binding (~ 1.625 Debye) at the transition.

Dilithium – For the dilithium molecule, we obtain a positron binding energy of 66.75(2) milliHartrees at an equilibrium bond length of 5.015 Bohr. The molecular binding energy of Li_2 from our calculations is ~ 38 milliHartrees, and the positron binding energy of a lone lithium atom is known from the literature to be ~ 2 milliHartrees [53], meaning this system is very stable against the $[\text{Li}_2, e^+] \rightarrow [\text{Li}, e^+] + \text{Li}$ dissociation channel. The one-particle density of the positronic ground-state of dilithium is shown in Fig. 2(a).

Benzene – The experimental positron binding energy of benzene is 5.51 milliHartrees [15]. Utilizing our variance-matching procedure (described in detail for benzene in the Supplementary Material), we obtain a finite positron binding energy of 4.1(3) milliHartrees. This falls in very close agreement with the binding energy obtained by Hofierka *et al.* of ~ 4.26 milliHartrees [47]. The one-particle density of the positronic ground-state of benzene is shown in Fig. 2(b).

Annihilation rates

The largest contribution to the annihilation process between positrons and electrons is the two-photon (2γ) annihilation rate, which is proportional to the positron-electron contact density. This quantity is readily obtained from our calculations. We have calculated 2γ positron annihilation rates (ac-

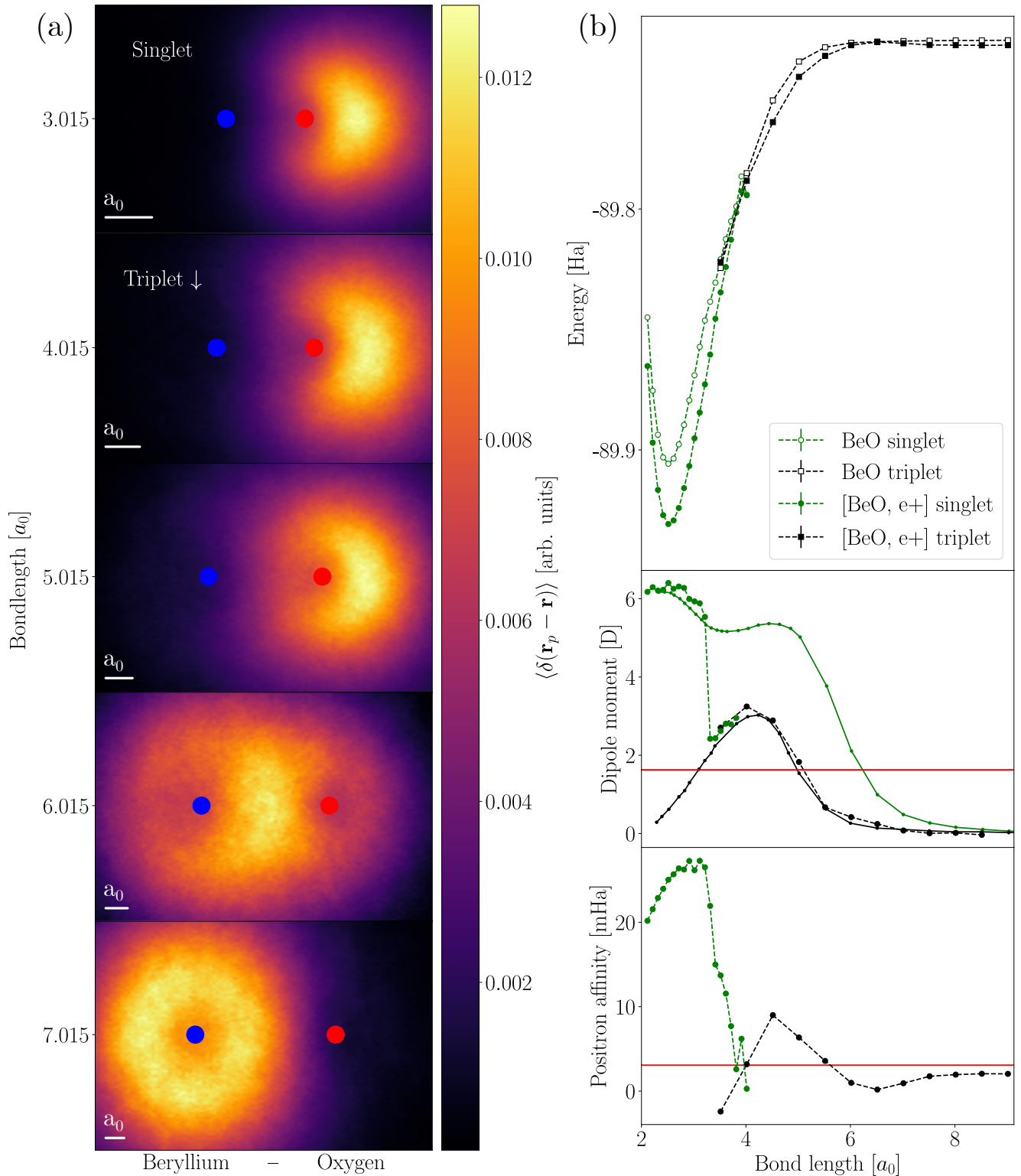


FIG. 1. **(a)** Ground-state positronic density, projected into the molecular plane, of a positron attached to a beryllium oxide molecule over a range of interatomic distances, accumulated via MCMC sampling. Image scale has been normalized by bondlength. The scale bar in the bottom left of each panel indicates the relative size of one Bohr radius, a_0 . The blue (red) marker indicates the position of the beryllium (oxygen) nucleus. **(b)** Energy (of the bare molecule and positronic complex), dipole moment (of the bare molecule), and positron binding energy of beryllium oxide over a range of interatomic distances. Green (black) markers in the dipole moment and positron binding energy plots indicate values accumulated for the electronic singlet (triplet) projected wavefunction. Error bars indicating standard errors in the Monte Carlo estimate of each quantity are smaller than the markers. Solid lines and dots in the dipole moment plot indicate the corresponding values obtained by Buenker *et al.* [29]. Horizontal red lines in the dipole moment and positron binding energy plots indicate the mean-field critical value for positron binding to the molecular dipole field and the positron affinity of a lone beryllium atom [52], respectively.

Method	LiH			BeO		
	Bare	Positronic	Binding energy	Bare	Positronic	Binding energy
FermiNet-VMC	-8.07051(1)	-8.10775(1)	0.03723(2)	-89.90572(4)	-89.93082(3)	0.02510(7)
SJ-VMC	-8.06307(3) [36]	-8.08034(4) [36]	0.01727(7)	-89.3173(25) [32]	-89.3365(13) [32]	0.0192(38)
SJ-FN-DMC	-8.070045(38) [36]	-8.10718(11) [36]	0.03714(15)	-89.7854(13) [32]	-89.8134(12) [32]	0.02800(25)
CISD	-8.03830 [25]	-8.05530 [25]	0.017	-	-	-
MRD-CI	-8.06827 [27]	-8.09764 [27]	0.02937	-89.759352 [29]	-89.773133 [29]	0.013781
ECG-SVM	-8.07054 [23]	-8.10747 [23]	0.03693	-	-	-
Hofierka <i>et al.</i> [47]	-	-	0.039(1)*[47]	-	-	-

* Theoretical (not statistical) uncertainty estimated from the comparison between different levels of theory as described by Hofierka *et al.*, caption of Table I

TABLE I. Ground state energy of LiH and BeO, and their positronic complexes, obtained via various computational methods at equilibrium bond-length. Statistical errors are omitted where they are smaller than the reported precision or otherwise omitted in the referenced source. The lowest variational energy in each column is bolded.

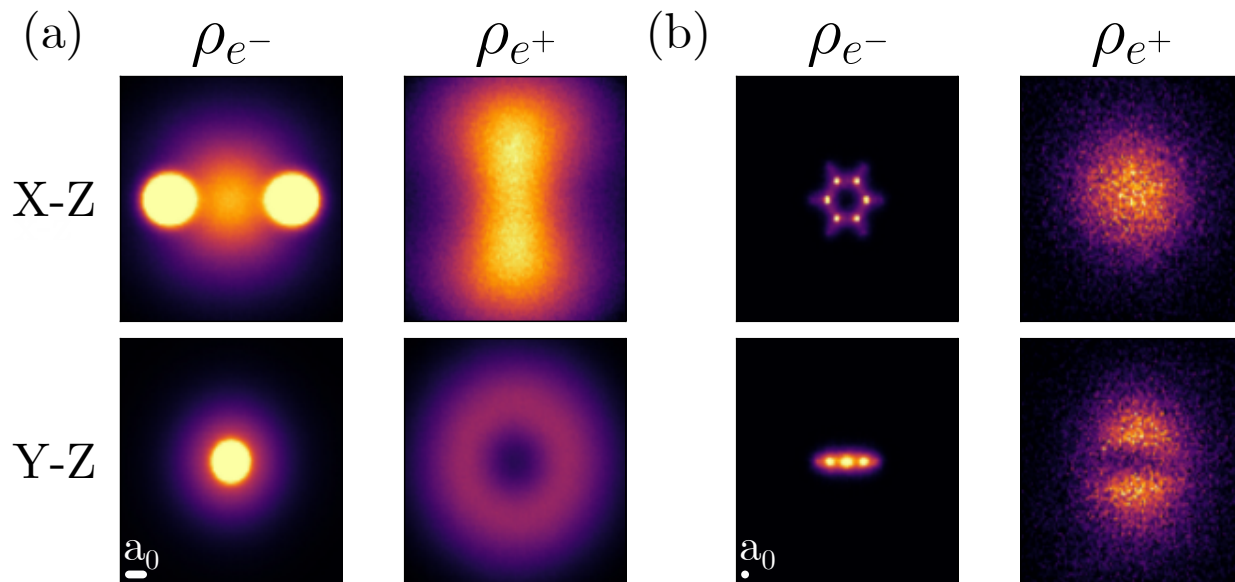


FIG. 2. Orthographic projections of the ground-state one-particle density for positronic (a) dilithium and (b) benzene molecules. Left/right columns show the electronic/positronic density, ρ_{e^-}/ρ_{e^+} . In the dilithium molecule, the positron is seen to be strongly localized to a torus wrapping the covalent bond. In the benzene molecule, the positronic orbital is highly diffuse, resulting in a much noisier Monte Carlo estimate of the one-particle density. The positronic orbital resembles a p -orbital ‘sandwiching’ the aromatic ring. The scale bar in the bottom left of each subfigure indicates the relative size of one Bohr radius, a_0 .

Method	HPs	2γ annihilation rate [ns^{-1}]					
		[Na ⁺ , Ps]	[Mg, e ⁺]	[LiH, e ⁺]	[BeO, e ⁺]	[Li ₂ , e ⁺]	[Benzene, e ⁺]
CI	2.0183 [26]	-	1.000991 [28]	0.8947* [31]	-	-	-
FN-DMC	2.32 [33]	-	-	1.3602* [34]	-	-	-
ECG-SVM	2.4361 [16], 2.4722 [17], 2.4685 [19]	1.898 [20]	0.955 [22], 1.0249 [28]	1.375 [23]	-	-	-
Hofierka <i>et al.</i> [47]	-	-	-	2.083	-	-	0.666
FermiNet-VMC	2.440(1)	1.870(1)	1.076(1)	1.3391(7)	0.9533(8)	1.962(2)	0.5247(6)

* Contact density at equilibrium bond length of 3.348 bohr obtained by quadratic interpolation of three values around the minimum in the potential energy surface.

TABLE II. 2γ annihilation rates for positronic atoms and molecules accumulated with FermiNet wavefunctions, compared with those obtained via various other computational methods. Statistical errors are omitted where they are smaller than the reported precision, or otherwise omitted in the referenced source. ECG results for all species besides HPs utilize the fixed-core approximation.

ording to the procedure detailed in the Supplementary Material) for every system studied, listed in Table II.

Positron annihilation rates are highly sensitive to the accurate description of the coalescence between the positron and electrons. This sensitivity, and the fact that annihilation rates are not a variational quantity, hinders the comparison between annihilation rates calculated by different methods. However, of the other methods compared in Table II, ECG-SVM captures this feature of the wavefunction best by construction. We see that our FermiNet-VMC annihilation rates are in close agreement with ECG-SVM results for positronium hydride, lithium hydride, and the alkali metal atoms. On this basis, we reason that our approach produces accurate annihilation rates, and therefore offers an accurate description of electron-positron correlations. We note that the many-body theory results of Hofierka *et al.* appear to overestimate the annihilation rate in lithium hydride compared to ECG-SVM, suggesting that FermiNet-VMC may be more suitable for the calculation of annihilation rates.

DISCUSSION

The selection of systems presented here spans a broad range of positron binding phenomena: positronium formation, binding with an induced atomic dipole moment, binding with a static molecular dipole moment, and binding due to correlations with covalent bonding electrons in molecules. In all cases where benchmarks are available, FermiNet-VMC produces excellent and, in some cases, state-of-the-art results for the positron binding energy. From the density plots presented, it is clear that this performance is consistent between wavefunctions with very different qualitative characteristics. An identical ansatz is used for every system studied – we have not employed any fine-tuning or system-specific treatments. An important aspect of our approach is that, due to being a basis-set-free method, we do not provide any information about the nature of the positron binding in the input to the calculation (e.g., via the placement of basis set functions). Rather, the location and nature of the positron binding emerges naturally during optimization of the wavefunction. The high level of accuracy achieved across various systems shows that FermiNet offers a flexible and accurate ansatz for mixed electron-positron wavefunctions.

To date, quantum Monte Carlo calculations of positron binding have focused on small, polar molecules. As pointed out by Hofierka *et al.* [47], accurate quantum Monte Carlo results for large non-polar organics, which comprise the majority of experimentally relevant systems, are lacking. We believe that the present work fills this gap. Our results for positronium hydride, sodium and magnesium atoms, and small diatomic molecules demonstrate that our approach can achieve state-of-the-art accuracy compared with previous work. Further, our results for the non-polar dilithium and benzene molecules demonstrate that this accuracy is retained when describing modes of positron binding governed entirely by strong electron-positron correlation effects. The results in Fig. 2 offer an intuitive understanding of the bind-

ing mechanism between non-polar molecules and positrons: correlation-dominated binding is facilitated by the presence of a centre of increased electronic density away from the atomic nuclei of a molecule. In dilithium, this is the covalent bond, and in benzene, this is the increased electronic density in the centre of the molecule from the delocalisation of the π -bonds in the ring.

Our result for the positron binding energy of benzene fall within ‘chemical accuracy’ (~ 1.6 milliHartrees) of the experimental value, but this level of accuracy is insufficient for other species of experimental interest. Many chemical species possess positron binding energies below chemical accuracy (see, e.g., the experimental binding energies in ref. [11], where 15 small organic molecules are found to possess binding energies below chemical accuracy), and obtaining this level of accuracy for relative energies represents a significant challenge to computational chemistry methods. We believe that the necessary improvement in accuracy, and obviation of our need to utilise variance matching, can be achieved by adopting the recently introduced PsiFormer architecture [54], an improvement upon the FermiNet architecture utilising Transformer networks [55], given that the PsiFormer obtains more accurate total energies for the ground-state energy of the bare benzene molecule than FermiNet.

As with previous work utilizing FermiNet, computational scaling remains an issue. Calculations involving $\gtrsim 50$ particles are too expensive for presently available computational resources, prohibiting the application of the method to large molecules. One approach to calculating the ground-state wavefunctions of large molecules is to utilize pseudopotentials to remove core electrons from the calculations. The positronic component of the wavefunction is often small near the atomic nuclei, so we would expect the correlation effect between the core electrons and the positron to be small. Pseudopotentials have been successfully employed in previous QMC calculations of positron lifetimes in solids [44]. As the architecture employed herein only extends the original FermiNet architecture to treat different particle types separately, we expect that future advances in the computational efficiency of FermiNet and related neural network wavefunctions will be able to be combined with our approach to model positron binding.

Finally, we highlight that these results demonstrate a general advantage of neural network wavefunction methods. The lack of a dependence on a basis set simplifies the treatment of systems which are not well described by traditional notions of atom-centered, low angular momentum basis functions. Highly accurate calculations can be carried out without foreknowledge of the appropriate features of the ground-state wavefunction, lowering the degree of inductive bias in the method. As a result, we believe that neural network variational Monte Carlo offers a highly performant, generic method for obtaining ground-state properties of any continuous-space Hamiltonian.

CONCLUSION

We have shown that the FermiNet ansatz for VMC calculations can be extended to include positrons naturally, treating positrons on an equal footing to electrons. Because this ansatz does not depend on a basis set, our treatment sidesteps traditional methods’ issues in selecting and converging an appropriate basis set for describing positronic wavefunctions. Our method produces highly accurate results for several molecules with various binding mechanisms for positrons without any system-specific tuning. We expect that the simplicity of this method will lend itself to many challenging applications beyond those presented here, e.g., calculations involving multiple positrons. With additional computational effort, this method can provide accurate predictions for positron annihilation experiments.

METHODS

We find the ground-state wavefunction and corresponding ground-state energy of the many-body Coulomb Hamiltonian in the Born-Oppenheimer clamped nuclei approximation,

$$\mathcal{H} = -\frac{1}{2} \sum_i \nabla_i^2 + \sum_{i,j} \frac{q_i Z_j}{|\mathbf{r}_i - \mathbf{R}_j|} + \sum_{i>j} \frac{q_i q_j}{|\mathbf{r}_i - \mathbf{r}_j|} + \sum_{i>j} \frac{Z_i Z_j}{|\mathbf{R}_i - \mathbf{R}_j|}, \quad (1)$$

where q_i, \mathbf{r}_i are the particle charges and positions, and Z_i, \mathbf{R}_i are the charges and positions of fixed nuclei. Here, and throughout, we utilise Hartree atomic units: $\hbar = e = m_e = 1$. For the mixed electron-positron systems considered here, $q_i = \pm 1$. We solve for the many-body ground-state wavefunction using the variational Monte Carlo (VMC) method: [56] a many-body wavefunction Ψ_θ , parameterized by θ , is continuously updated via a gradient descent procedure to minimize the energy expectation value,

$$\langle E \rangle_\theta = \frac{\int \Psi_\theta^*(\mathbf{r}) \mathcal{H} \Psi_\theta(\mathbf{r}) d\mathbf{r}}{\int \Psi_\theta^*(\mathbf{r}) \Psi_\theta(\mathbf{r}) d\mathbf{r}}, \quad (2)$$

where $\mathbf{r} = (\mathbf{r}_1, \dots, \mathbf{r}_N)$. This integral, and its gradient with respect to θ , are evaluated via Monte Carlo integration. Particle configurations, $\mathbf{r}^{(i)}$, are sampled from the probability density $|\Psi_\theta(\mathbf{r})|^2$ via the Metropolis-Hastings algorithm. The expectation value of the energy and its gradient are then evaluated by the Monte Carlo estimators,

$$\langle E \rangle_\theta = \lim_{N \rightarrow \infty} \left[\frac{1}{N} \sum_{i=1}^N \frac{\mathcal{H} \Psi_\theta(\mathbf{r}^{(i)})}{\Psi_\theta(\mathbf{r}^{(i)})} \right] = \mathbb{E}_{\mathbf{r} \sim |\Psi_\theta|^2} \left[\frac{\mathcal{H} \Psi_\theta(\mathbf{r})}{\Psi_\theta(\mathbf{r})} \right] \quad (3)$$

$$\nabla_\theta \langle E \rangle_\theta = 2 \mathbb{E}_{\mathbf{r} \sim |\Psi_\theta|^2} \left[\left(\frac{\mathcal{H} \Psi_\theta(\mathbf{r})}{\Psi_\theta(\mathbf{r})} - \langle E \rangle_\theta \right) \nabla_\theta \log |\Psi_\theta(\mathbf{r})| \right] \quad (4)$$

The FermiNet represents the many-body wavefunction as a sum of block-diagonal determinants containing many-particle functions which depend upon the coordinates of all particles

in a permutation equivariant manner. This is written

$$\Psi(\mathbf{r}) = \sum_k \prod_\chi \det \left[\psi_i^{k\chi}(\mathbf{r}_j^\chi; \{\mathbf{r}_{/j}^\chi\}; \{\mathbf{r}_j^{\prime\chi}\}) \right], \quad (5)$$

where the set $\{\mathbf{r}_{/j}\}$ includes all particle coordinates except \mathbf{r}_j , and $\chi = (\sigma, q)$ labels species of particles which are distinguished by their spin $\sigma \in (\uparrow, \downarrow)$ and charge $q \in (+, -)$. Here we have made a slight abuse of notation for the sake of brevity: permutation invariance for the set $\{\mathbf{r}_j^{\prime\chi}\}$ is only maintained between particles of the same species. We emphasise that these are not the dense determinants discussed in recent works extending FermiNet [57], except the benzene calculation for which dense determinants were used for the electronic component of the wavefunction. The many-particle functions ψ_i are represented by a deep neural network [48] (architecture described in the Supplementary Material). Multiplicative coefficients are omitted from the sum as they are trivially absorbed into the entries of the determinant. Gradient descent is performed via the Kronecker-factored approximate curvature (KFAC) algorithm, an approximation of natural gradient descent [58] which scales well to large neural networks [59]. Natural gradient descent is closely related to the stochastic reconfiguration method, well-known in the quantum Monte Carlo literature [60]. The present work introduces two alterations to the original FermiNet architecture. Firstly, we have included positronic orbitals as additional species, i.e. additional blocks in the determinant. Secondly, we utilise distinct weights in the neural network layers for every species (unlike the original FermiNet, where spin up and down electronic orbitals shared weights).

A single determinant of the form in Eq. (5) can represent any fermionic many-body wavefunction [61]. In practice, the argument for the universality of FermiNet determinants depends upon the representation of discontinuous functions which cannot be constructed using realistic neural networks. Despite this, FermiNet-VMC calculations obtain state-of-the-art accuracy in ground state energy calculations for a range of molecules and solids [48, 49, 57, 62–64] with a linear combination of a small number of determinants. We utilise 32 determinants for all calculations in the present work.

We only consider calculations involving a single positron in the present work. We have discussed the treatment of the positronic spin coordinate only to demonstrate how our technique may be extended to calculations involving many positrons, as such systems have recently attracted theoretical interest.

Ground-state wavefunctions for bare and positronic molecules are not guaranteed to be similarly converged after an equal number of gradient descent steps. This introduces uncontrolled error in calculating positron binding energies via VMC. Previous work has shown that FermiNet-VMC calculations yield ground-state energies within chemical accuracy (~ 1.5 milliHartrees) of exact results for many small molecules [48, 49]. With this level of accuracy, the uncontrolled error will be negligible for molecules with a large positron binding energy. However, for molecules with very small binding energies, or large molecules for which the uncontrolled error may become large compared to the positron

binding energy, there is no guarantee that an accurate estimate of the positron binding energy will be obtained by comparing ground-state calculations of different quality. In these cases, we employ the variance matching technique described by Entwistle *et al.* [65], addressed in the Supplementary Material.

ACKNOWLEDGMENTS

This work was undertaken with funding from the UK Engineering and Physical Sciences Research Council (EP/T51780X/1) (GC). Calculations were carried out with resources provided by the Baskerville Accelerated Compute

Facility through a UK Research and Innovation Access to HPC grant. Additionally, the authors gratefully acknowledge both PRACE, and the Gauss Centre for Supercomputing e.V. (www.gauss-centre.eu) for funding this project by providing computing time through the John von Neumann Institute for Computing (NIC) on the GCS Supercomputer JUWELS at Jülich Supercomputing Centre (JSC). Via his membership of the UK's HEC Materials Chemistry Consortium, which is funded by EPSRC (EP/R029431), Foulkes used the UK Materials and Molecular Modelling Hub for computational resources, MMM Hub, which is partially funded by EPSRC (EP/T022213).

-
- [1] P. A. M. Dirac and R. H. Fowler, *Proc. R. Soc. A* **117**, 610 (1928).
- [2] A. K. Shukla and U. Kumar, *J Med Phys* **31**, 13 (2006).
- [3] N. Prantzios, C. Boehm, A. M. Bykov, R. Diehl, K. Ferrière, N. Guessoum, P. Jean, J. Knoedseder, A. Marcowith, I. V. Moskalenko, A. Strong, and G. Weidenspointner, *Rev. Mod. Phys.* **83**, 1001 (2011).
- [4] F. Tuomisto and I. Makkonen, *Rev. Mod. Phys.* **85**, 1583 (2013).
- [5] C. Hugenschmidt, *Surface Science Reports* **71**, 547 (2016).
- [6] C. M. Surko, *Nature* **449**, 153 (2007).
- [7] S. J. Gilbert, L. D. Barnes, J. P. Sullivan, and C. M. Surko, *Phys. Rev. Lett.* **88**, 043201 (2002).
- [8] L. D. Barnes, S. J. Gilbert, and C. M. Surko, *Phys. Rev. A* **67**, 032706 (2003).
- [9] L. D. Barnes, J. A. Young, and C. M. Surko, *Phys. Rev. A* **74**, 012706 (2006).
- [10] J. A. Young and C. M. Surko, *Phys. Rev. A* **77**, 052704 (2008).
- [11] J. A. Young and C. M. Surko, *Phys. Rev. A* **78**, 032702 (2008).
- [12] J. R. Danielson, J. A. Young, and C. M. Surko, *J. Phys. B: At. Mol. Opt. Phys.* **42**, 235203 (2009).
- [13] J. R. Danielson, J. J. Gosselin, and C. M. Surko, *Phys. Rev. Lett.* **104**, 233201 (2010).
- [14] J. R. Danielson, A. C. L. Jones, M. R. Natisin, and C. M. Surko, *Phys. Rev. Lett.* **109**, 113201 (2012).
- [15] G. F. Gribakin, J. A. Young, and C. M. Surko, *Rev. Mod. Phys.* **82**, 2557 (2010).
- [16] A. M. Frolov and V. H. Smith, *Phys. Rev. A* **55**, 2662 (1997).
- [17] J. Usukura, K. Varga, and Y. Suzuki, *Phys. Rev. A* **58**, 1918 (1998).
- [18] J. Mitroy and G. G. Ryzhikh, *J. Phys. B: At. Mol. Opt. Phys.* **32**, L621 (1999).
- [19] G. G. Ryzhikh and J. Mitroy, *Journal of Physics B: Atomic, Molecular and Optical Physics* **32**, 4051 (1999).
- [20] G. G. Ryzhikh, J. Mitroy, and K. Varga, *Journal of Physics B: Atomic, Molecular and Optical Physics* **31**, 3965 (1998).
- [21] J. Mitroy and G. G. Ryzhikh, *Journal of Physics B: Atomic, Molecular and Optical Physics* **33**, 3495 (2000).
- [22] J. Mitroy and G. G. Ryzhikh, *Journal of Physics B: Atomic, Molecular and Optical Physics* **34**, 2001 (2001).
- [23] K. Strasburger, *J. Chem. Phys.* **114**, 615 (2001).
- [24] S. Bubin and L. Adamowicz, *The Journal of Chemical Physics* **120**, 6051 (2004).
- [25] K. Strasburger, *Chemical Physics Letters* **253**, 49 (1996).
- [26] M. Bromley, J. Mitroy, and G. Ryzhikh, *Nuclear Instruments and Methods in Physics Research Section B: Beam Interactions with Materials and Atoms* **171**, 47 (2000).
- [27] R. J. Buenker, H.-P. Liebermann, V. Melnikov, M. Tachikawa, L. Pichl, and M. Kimura, *J. Phys. Chem. A* **109**, 5956 (2005).
- [28] M. W. J. Bromley and J. Mitroy, *Phys. Rev. A* **73**, 032507 (2006).
- [29] R. J. Buenker, H.-P. Liebermann, L. Pichl, M. Tachikawa, and M. Kimura, *J. Chem. Phys.* **126**, 104305 (2007).
- [30] R. J. Buenker and H.-P. Liebermann, *Nuclear Instruments and Methods in Physics Research Section B: Beam Interactions with Materials and Atoms* **266**, 483 (2008), low Energy Positron and Positronium Physics.
- [31] R. J. Buenker and H.-P. Liebermann, *Nuclear Instruments and Methods in Physics Research Section B: Beam Interactions with Materials and Atoms* **267**, 763 (2009).
- [32] D. Bressanini, M. Mella, and G. Morosi, *J. Chem. Phys.* **109**, 1716 (1998).
- [33] M. Mella, G. Morosi, and D. Bressanini, *The Journal of Chemical Physics* **111**, 108 (1999).
- [34] M. Mella, S. Chiesa, and G. Morosi, *The Journal of Chemical Physics* **116**, 2852 (2002).
- [35] Y. Kita, R. Maezono, and M. Tachikawa, in *Recent Progress in Computational Sciences and Engineering* (CRC Press, 2006).
- [36] Y. Kita, R. Maezono, M. Tachikawa, M. Towler, and R. J. Needs, *J. Chem. Phys.* **131**, 134310 (2009).
- [37] Y. Kita, R. Maezono, M. Tachikawa, M. D. Towler, and R. J. Needs, *J. Chem. Phys.* **135**, 054108 (2011).
- [38] S. Ito, D. Yoshida, Y. Kita, and M. Tachikawa, *J. Chem. Phys.* **153**, 224305 (2020).
- [39] D. Bressanini, *J. Chem. Phys.* **155**, 054306 (2021).
- [40] J. A. Charry Martinez, M. Barborini, and A. Tkatchenko, *J. Chem. Theory Comput.* **18**, 2267 (2022).
- [41] E. Boroński and R. M. Nieminen, *Phys. Rev. B* **34**, 3820 (1986).
- [42] J. Kuriplach and B. Barbiellini, *Phys. Rev. B* **89**, 155111 (2014).
- [43] N. D. Drummond, P. López Ríos, R. J. Needs, and C. J. Pickard, *Phys. Rev. Lett.* **107**, 207402 (2011).
- [44] K. A. Simula, J. E. Muff, I. Makkonen, and N. D. Drummond, *Phys. Rev. Lett.* **129**, 166403 (2022), arXiv:2202.13204 [cond-mat].
- [45] D. Schrader, *Nuclear Instruments and Methods in Physics Research Section B: Beam Interactions with Materials and Atoms* **143**, 209 (1998).
- [46] M. W. J. Bromley, *Positron-atom interactions studied using configuration interaction methods* (Charles Darwin University (Australia), 2002).

- [47] J. Hofierka, B. Cunningham, C. M. Rawlins, C. H. Patterson, and D. G. Green, *Nature* **606**, 688 (2022).
- [48] D. Pfau, J. S. Spencer, A. G. D. G. Matthews, and W. M. C. Foulkes, *Phys. Rev. Research* **2**, 033429 (2020).
- [49] J. S. Spencer, D. Pfau, A. Botev, and W. M. C. Foulkes, arXiv:2011.07125 [physics] (2020), 2011.07125 [physics].
- [50] H. Flyvbjerg and H. G. Petersen, *J. Chem. Phys.* **91**, 7 (1989).
- [51] G. Ryzhikh, J. Mitroy, and K. Varga, *Journal of Physics B: Atomic, Molecular and Optical Physics* **31**, L265 (1998).
- [52] M. W. J. Bromley and J. Mitroy, *Phys. Rev. A* **65**, 012505 (2001).
- [53] J. Mitroy, M. W. J. Bromley, and G. G. Ryzhikh, *J. Phys. B: At. Mol. Opt. Phys.* **35**, R81 (2002).
- [54] I. von Glehn, J. S. Spencer, and D. Pfau, “A Self-Attention Ansatz for Ab-initio Quantum Chemistry,” (2022), arXiv:2211.13672 [physics].
- [55] A. Vaswani, N. Shazeer, N. Parmar, J. Uszkoreit, L. Jones, A. N. Gomez, Ł. Kaiser, and I. Polosukhin, in *Advances in Neural Information Processing Systems*, Vol. 30 (Curran Associates, Inc., 2017).
- [56] W. M. C. Foulkes, L. Mitas, R. J. Needs, and G. Rajagopal, *Rev. Mod. Phys.* **73**, 33 (2001).
- [57] G. Cassella, H. Sutterud, S. Azadi, N. Drummond, D. Pfau, and J. S. Spencer, *Phys. Rev. Letters* **130**, 036401 (2023).
- [58] S.-i. Amari, *Neural Computation* **10**, 251 (1998).
- [59] J. Martens and R. Grosse, *Proceedings of the 32nd International Conference on Machine Learning*, PMLR **37**, 2408 (2015).
- [60] S. Sorella, *Phys. Rev. B* **71**, 241103 (2005).
- [61] M. Hutter, arXiv:2007.15298 (2020).
- [62] M. Wilson, S. Moroni, M. Holzmann, N. Gao, F. Wudarski, T. Vegge, and A. Bhowmik, *Phys. Rev. B* **107**, 235139 (2023).
- [63] M. Wilson, N. Gao, F. Wudarski, E. Rieffel, and N. M. Tubman, arXiv:2103.12570 (2021).
- [64] X. Li, C. Fan, W. Ren, and J. Chen, *Phys. Rev. Research* **4**, 013021 (2022).
- [65] M. Entwistle, Z. Schätzle, P. A. Erdman, J. Hermann, and F. Noé, arXiv:2203.09472 (2022).
- [66] T. Kato, *Comm. Pure Appl. Math.* **10**, 151 (1957).
- [67] J. C. Kimball, *Phys. Rev. A* **7**, 1648 (1973).
- [68] J. Bradbury, R. Frostig, P. Hawkins, M. J. Johnson, C. Leary, D. Maclaurin, G. Necula, A. Paszke, J. VanderPlas, S. Wanderman-Milne, and Q. Zhang, “JAX: composable transformations of Python+NumPy programs,” <http://github.com/google/jax> (2018).
- [69] D. Pfau and J. Spencer, “Ferminet JAX implementation,” <http://github.com/deepmind/ferminet> (2020).
- [70] A. Botev, “KFAC JAX implementation,” https://github.com/deepmind/deepmind-research/tree/master/kfac_ferminet_alpha (2020).

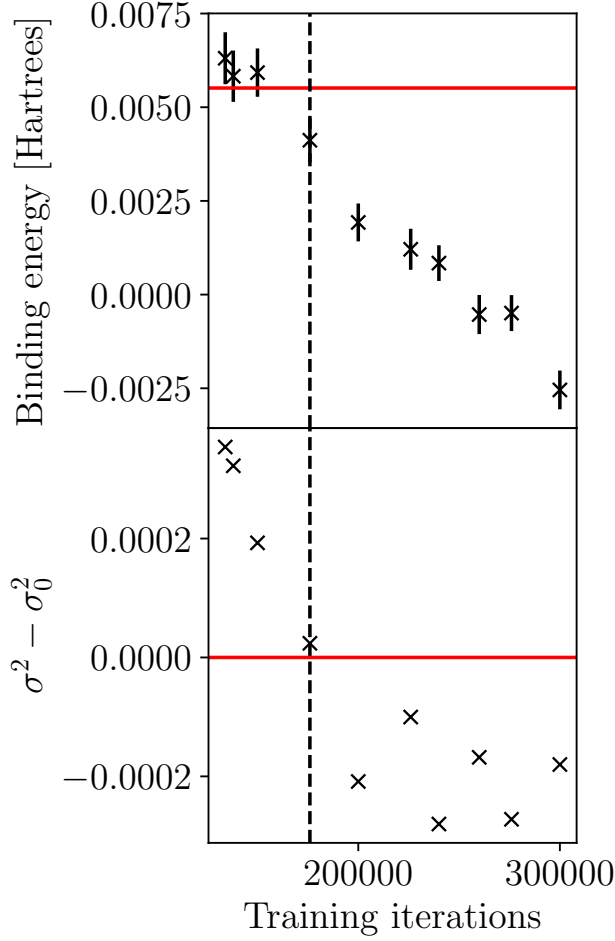


FIG. 3. **Top:** Binding energy obtained using bare molecular ground-state energies obtained from checkpoints taken after varying training iterations. **Bottom:** Local energy variance difference between bare molecular checkpoints and positronic molecule at the end of training.

APPENDICES

Variance matching

Variance matching was utilised in the main text to calculate the positron binding energy for the sodium atom and the benzene molecule. Here we will describe the procedure for obtaining benzene’s positron binding energy. We note that all variances are evaluated by freezing the wavefunction parameters and taking 10k samples of the local energy by MCMC sampling. The variance in the local energy is calculated using a reblocking procedure to account for sequential correlations in the MCMC sampling [50].

After a fixed number of optimisation steps (i.e. at the end of training), we calculate the variance of the local energy for the positronic ground-state wavefunction. We then calculate the variance of the local energy for the bare molecular ground-state wavefunction at a series of regularly spaced

checkpoints during training – approximately every 50k iterations from 150k to 300k. We refine the variance matching by calculating the variance between the two checkpoints where the difference crosses zero. We additionally calculate the variance at several other randomly chosen points in the range of interest to validate our implicit assumption that the variance is approximately monotonic. The closest variance match is obtained after 175k training iterations of the bare molecule. The binding energy and variance difference as a function of the bare molecule training iterations is shown in Fig. 3. The obtained variance difference as a function of training iteration is not completely monotonic due to the stochastic optimisation procedure.

Fermionic neural networks

The many-body orbitals $\Psi_i^{k\chi}$, which enter into FermiNet determinants (Eq. (5)), are represented by a deep neural network architecture. Electron-nuclear and electron-electron coordinates are input to the network. The vector separations and their norms are used as inputs: the norm provides the necessary discontinuity to allow the – otherwise smooth – network to satisfy the Kato cusp conditions [66]. We write these inputs as

$$\mathbf{h}_i^{l\chi} = (\mathbf{r}_i^\chi - \mathbf{R}_I, \|\mathbf{r}_i^\chi - \mathbf{R}_I\| \quad \forall \quad I) \quad (6)$$

$$\mathbf{h}_{ij}^{l\chi\xi} = (\mathbf{r}_i^\chi - \mathbf{r}_j^\xi, \|\mathbf{r}_i^\chi - \mathbf{r}_j^\xi\|), \quad (7)$$

with the notation in brackets indicating the concatenation of the vector separation and its norm for all pairs of indices, \mathbf{R}_I referring to nuclear co-ordinates, χ and ξ labelling fermionic species as in the main text, and $\|\cdot\|$ the Euclidean norm.

Consecutive transformations update these input features,

$$\mathbf{h}_i^{l+1\chi} = \tanh(\underline{\mathbf{V}}^l \mathbf{j}_i^{l\chi} + \mathbf{b}^l) + \mathbf{h}_i^{l\chi} \quad (8)$$

$$\mathbf{h}_{ij}^{l+1\chi\xi} = \tanh(\underline{\mathbf{W}}^l \mathbf{h}_{ij}^{l\chi\xi} + \mathbf{c}^l) + \mathbf{h}_{ij}^{l\chi\xi}. \quad (9)$$

where

$$\mathbf{j}_i^{l\chi} = \text{concatenate}(\mathbf{h}_i^{l\chi}, \mathbf{H}_i^{l\chi}) \quad (10)$$

and

$$\mathbf{H}_i^{l\chi} = \text{concatenate}_\xi \left(\frac{1}{n^\xi} \sum_{j=1}^{n^\xi} \mathbf{h}_j^{l\xi}, \frac{1}{n^\xi} \sum_{j=1}^{n^\xi} \mathbf{h}_{ij}^{l\chi\xi} \right). \quad (11)$$

The first transformation (one subscripted index) is referred to as the one-electron stream, and the second (two subscripted indices) is the two-electron stream. These are the ‘layers’ of the network. The linear dimension of the weight matrices $\underline{\mathbf{V}}^l$ and $\underline{\mathbf{W}}^l$ determine the ‘width’ of the layers. These widths, and the total number of layers L , are the hyperparameters which determine the network architecture.

The outputs from the L^{th} transformation are subject to a final, spin-dependent, linear transformation and multiplied by

(in open boundary conditions) an exponentially decaying envelope [49], which enforces the decay of the wave function as $r_i \rightarrow \infty$,

$$\psi_i^{k\chi}(\mathbf{r}_j, \{\mathbf{r}_{/j}\}) = \phi_i^{k\chi}(\mathbf{r}_j, \{\mathbf{r}_{/j}\}) f_i^{k\chi}(\mathbf{r}_j) \quad (12)$$

where

$$\phi_i^{k\chi}(\mathbf{r}_j, \{\mathbf{r}_{/j}\}) = (\mathbf{w}_i^{k\chi} \cdot \mathbf{h}_j^{L\chi} + g_i^{k\chi}) \quad (13)$$

and

$$f_i^{k\chi}(\mathbf{r}_j) = \left[\sum_m \pi_{im}^{k\chi} \exp\left(-\sigma_{im}^{k\chi} |(\mathbf{r}_j^\chi - \mathbf{R}_m)|\right) \right]. \quad (14)$$

The functions $\psi_i^{k\chi}$ are used as the inputs to the determinants, Eq. (5).

The determinant expansion in Eq. (5) does not require multiplicative coefficients as they can be trivially absorbed into the determinants [49]. Hutter showed that a single determinant of such many-body functions could represent any anti-symmetric function [61]. However, the proof depends upon the construction of discontinuous functions that cannot be represented in practice by a finite network of a reasonable size.

The set of parameters,

$$\theta = \{\underline{\mathbf{V}}^l, \underline{\mathbf{W}}^l, \mathbf{w}_i^{k\chi}, \mathbf{b}^l, \mathbf{c}^l, g_i^{k\chi}, \pi_{im}^{k\chi}, \sigma_{im}^{k\chi}\}, \quad (15)$$

are all learnable. The electronic orbitals, $\chi = (\sigma, -)$, are pre-trained to the Hartree-Fock orbitals of the bare molecule, even for positronic calculations, according to the procedure outlined in [48]. For a more extensive description of the FermiNet architecture, see Pfau *et al.* [48].

Calculating annihilation rates with VMC

We follow the procedure for the calculation of positron annihilation rates within the VMC framework described in ref. [44], which we repeat here. The dominant process for positron annihilation in molecular bound states is the 2γ annihilation, which is proportional to the expectation value of the spin-projected contact density between positrons and electrons. The 2γ annihilation rate is thus calculated as,

$$\Gamma = \pi r_0^2 c \sum_{i=1}^N \frac{\langle \Psi | \hat{O}_i^s \delta(\mathbf{r}_i - \mathbf{r}_+) | \Psi \rangle}{\langle \Psi | \Psi \rangle} = 100.9 g(0) \quad (16)$$

where \mathbf{r}_i is the position of the i^{th} of N electrons, \mathbf{r}_+ is the position of the positron, \hat{O}_i^s is the spin projection operator to the positron-electron singlet for electron i , r_0 is the classical electron radius, c is the speed of light, and the prefactor has been expressed such that the final expression is given in units of ns^{-1} .

The rotationally and translationally averaged pair correlation function $g(r)$ is calculated as

$$g(r) dr = \frac{1}{2} \mathbb{E}_{\mathbf{r} \sim |\Psi|^2} \left[\frac{\sum_{i=1}^N \delta(|\mathbf{r}_i - \mathbf{r}_+| - r)}{4\pi r^2} \right] \quad (17)$$

Kind	Parameter	Value
Network	Number of determinants	32
Network	One-particle stream width	512
Network	Two-particle stream width	32
Optim	Batch size	4096
Optim	Training iterations	3e5
Optim	Pretraining iterations	1e4
Optim	Learning rate	$(1e4 + t)^{-1}$
Optim	Local energy clipping	5.0
KFAC	Momentum	0
KFAC	Covariance moving average decay	0.95
KFAC	Norm constraint	1e-3
KFAC	Damping	1e-3
MCMC	Steps between parameter updates	10

TABLE III. FermiNet hyperparameters for all experiments in the paper. For the Benzene calculations, the decay of the learning rate was disabled (i.e. the value was fixed at 1e-4 throughout training)

where the prefactor of 1/2 enacts the averaging over spin species resulting from the action of the spin projection operator.

In practice this is accumulated by sampling electron and positron positions from $|\Psi|^2$ via the Metropolis-Hastings algorithm. Electron-positron separations are accumulated into fixed-width bins, which are then normalized to produce a histogram of values of $g(r)$. We fit $\log g(r)$ to a fifth-order polynomial via the Levenberg-Marquadt algorithm as implemented in SciPy, excluding bins with zero counts, and extrapolate the value to $r = 0$ to evaluate $g(0)$. The first-order term in the polynomial is fixed to $-x$ to satisfy the Kimball cusp conditions [67]. Extrapolation is necessary due to the vanishing volume of the spherical bins for separations approaching $r = 0$. Errors in the bin counts are estimated as

$$\sigma_r \simeq \sqrt{C_r} \quad (18)$$

where C_r is the number of counts in a bin centered at r . The error in $g(0)$ is obtained from the variance of the 0th order parameter of the polynomial fit.

Experimental setup

Four A100 GPUs were used for all calculations presented, except the Benzene molecule, for which sixteen A100 GPUs were used. Single-precision floating point numbers were used in all calculations. The FermiNet was implemented using the JAX Python library [68], extending a development version of the FermiNet [69]. Optimization used a JAX implementation of the Kronecker-factored approximate curvature (KFAC) gradient descent algorithm [49, 59, 70].

Monte Carlo moves are accepted/rejected on a per-species basis, including spin species. All particles of a given species are moved simultaneously within each Monte Carlo step. Each species has an independent Monte Carlo step proposal size, and this step size is adapted during training to maintain a $\sim 50\%$ acceptance rate.

We found the convergence of the Benzene calculations was accelerated when the decay of the learning rate (see Table III)

was disabled. We found that following this aggressive training regime with an additional 2000 training iterations with the appropriately decayed learning rate greatly improved the energies obtained during inference. Understanding the training dynamics of the FermiNet continues to be an open question of great interest.

DATA TABLES

Lithium hydride

Bondlength [a_0]	Energy [Hartrees]			
	Bare	σ_{Bare}	Positronic	$\sigma_{\text{Positronic}}$
2.815	-8.069021	0.000004	-8.100914	0.000004
2.882	-8.069882	0.000005	-8.102727	0.000009
2.948	-8.070345	0.000003	-8.104151	0.000010
3.015	-8.070507	0.000004	-8.105283	0.000004
3.082	-8.070371	0.000007	-8.106226	0.000007
3.148	-8.069958	0.000003	-8.106885	0.000005
3.215	-8.069331	0.000004	-8.107324	0.000003
3.281	-8.068203	0.000278	-8.107583	0.000003
3.348	-8.067207	0.000287	-8.107737	0.000004
3.415	-8.066352	0.000007	-8.107712	0.000011
3.481	-8.065065	0.000005	-8.107542	0.000004
3.548	-8.063663	0.000005	-8.107234	0.000005
3.615	-8.062156	0.000004	-8.106949	0.000006
3.682	-8.060571	0.000004	-8.106551	0.000008
3.749	-8.058894	0.000008	-8.105952	0.000010
3.816	-8.057171	0.000005	-8.105373	0.000132
3.883	-8.055407	0.000007	-8.104972	0.000006
3.950	-8.053575	0.000007	-8.104321	0.000010
4.017	-8.051748	0.000008	-8.103593	0.000004
4.084	-8.049849	0.000008	-8.102936	0.000005
4.151	-8.047965	0.000005	-8.102246	0.000010

Beryllium oxide

Bondlength [a_0]	Energy [Hartrees]			
	Bare	σ_{Bare}	Positronic	$\sigma_{\text{Positronic}}$
			Singlet	
2.115	-89.845004	0.000024	-89.865185	0.000027
2.215	-89.875412	0.000024	-89.896963	0.000019
2.315	-89.893706	0.000014	-89.916586	0.000019
2.415	-89.903115	0.000042	-89.927073	0.000033
2.515	-89.905721	0.000014	-89.930761	0.000057
2.615	-89.903574	0.000075	-89.929260	0.000088
2.715	-89.897711	0.000070	-89.924101	0.000020
2.815	-89.889610	0.000022	-89.915860	0.000043
2.915	-89.879387	0.000073	-89.906657	0.000029
3.015	-89.869008	0.000073	-89.895173	0.000032
3.115	-89.857212	0.000018	-89.884496	0.000039
3.215	-89.846269	0.000021	-89.872785	0.000118
3.315	-89.838491	0.000082	-89.860431	0.000095
3.415	-89.830544	0.000024	-89.845536	0.000027
3.515	-89.820883	0.000027	-89.834588	0.000032
3.615	-89.812532	0.000032	-89.824085	0.000029
3.715	-89.805062	0.000019	-89.812757	0.000077
3.815	-89.798934	0.000097	-89.801516	0.000026
3.915	-89.786483	0.000030	-89.792682	0.000042
4.015	-89.794044	0.000051	-89.794320	0.000043
			Triplet	
3.515	-89.824472	0.000018	-89.822049	0.000031
4.015	-89.784895	0.000023	-89.788294	0.000031
4.515	-89.754943	0.000024	-89.763941	0.000031
5.015	-89.738802	0.000023	-89.745154	0.000032
5.515	-89.732889	0.000022	-89.736450	0.000033
6.015	-89.731046	0.000022	-89.732024	0.000033
6.515	-89.730538	0.000023	-89.730718	0.000034
7.015	-89.730307	0.000022	-89.731238	0.000031
7.515	-89.730150	0.000021	-89.731904	0.000030
8.015	-89.730040	0.000021	-89.731992	0.000036
8.515	-89.730035	0.000025	-89.732091	0.000031
9.015	-89.729969	0.000022	-89.732011	0.000030

Benzene

System	$\langle E \rangle$ [Hartrees]	σ_E^2
Positronic @ 300k iter.	-232.223293	0.000847
Bare @ 134k iter.	-232.216986	0.001202
Bare @ 138k iter.	-232.217466	0.001170
Bare @ 150k iter.	-232.217369	0.001040
Bare @ 176k iter.	-232.219174	0.000871
Bare @ 200k iter.	-232.221368	0.000639
Bare @ 226k iter.	-232.222084	0.000747
Bare @ 240k iter.	-232.222453	0.000568
Bare @ 260k iter.	-232.223825	0.000680
Bare @ 276k iter.	-232.223786	0.000576
Bare @ 300k iter.	-232.225837	0.000668